Applied Catalysis A: General 506 (2015) 278–287

Contents lists available at ScienceDirect

Applied Catalysis A: General

journal homepage: www.elsevier.com/locate/apcata

Effect of reduction temperature on the characteristics and catalytic properties of TiO_2 supported AuPd alloy particles prepared by one-step flame spray pyrolysis in the selective hydrogenation of 1-heptyne

Boontida Pongthawornsakun[a], Okorn Mekasuwandumrong[b], Swamy Prakash[c], Eric Ehret[c], Francisco J. Cadete Santos Aires[c], Joongjai Panpranot[a,*]

[a] Center of Excellence on Catalysis and Catalytic Reaction Engineering, Department of Chemical Engineering, Faculty of Engineering, Chulalongkorn University, Bangkok 10330, Thailand
[b] Department of Chemical Engineering, Faculty of Engineering and Industrial Technology, Silpakorn University, Nakorn Pathom 73000, Thailand
[c] Institut de Recherches sur la Catalyse et l'Environnement de Lyon—IRCELYON (UMR 5256CNRS/Univ. Lyon I), 2 Avenue Albert Einstein, 69626 Villeurbanne Cedex, France

ARTICLE INFO

Article history:
Received 29 April 2015
Received in revised form 8 September 2015
Accepted 9 September 2015
Available online 11 September 2015

Keywords:
Flame spray pyrolysis
$AuPd/TiO_2$
1-Heptyne
Selective hydrogenation

ABSTRACT

The bimetallic flame spray-synthesized $AuPd/TiO_2$ catalysts (Au:Pd weight ratio 1:1) were reduced for 2 h under H_2 at two different temperatures (40 °C and 500 °C) and tested in the liquid phase selective hydrogenation of 1-heptyne under mild conditions (30 °C and 4 bar H_2). Based on TEM-EDX analysis of individual nanoparticles, reduction at 500 °C tends to homogenize the composition of the individual AuPd nanoparticles without significant changes of their average particle size and bulk composition. Higher reaction rate (245 μmol s^{-1} g $cat.^{-1}$) was obtained on the $AuPd/TiO_2$ R40 than on the $AuPd/TiO_2$ R500 (223 μmol s^{-1} g $cat.^{-1}$). Upon reduction at 500 °C, the bimetallic $AuPd/TiO_2$ exhibited a similar degree of the strong-metal support interaction (SMSI) effect as the monometallic one. As revealed by XPS results, the ratios of Pd/Ti on both catalysts decreased by ca. 23%, due probably to the migration of TiO_x species onto the metals. The highest yield of 1-heptene (~93%) was obtained over the bimetallic $AuPd/TiO_2$ reduced at 40 °C in 20 min reaction time under the reaction conditions used. The high temperature reduction is unnecessary for the improvement of catalyst performances when using supported bimetallic AuPd catalysts.

1. Introduction

Flame aerosol synthesis, especially flame spray pyrolysis (FSP) is one of the interesting methods of nanoparticle production and is also a beneficial catalyst synthesis technique because the catalysts can easily be prepared in one-step without post-treatment steps such as washing, drying, filtration, and calcination. FSP synthesis has been employed for the synthesis of TiO_2 supported monometallic Au and Pd catalysts [1–3]; meanwhile, bimetallic AuPd supported on TiO_2 nanoparticles were successfully synthesized by the single-step FSP in our recent study [4]. Formation of Au–Pd alloy bimetallic nanoparticles was evidenced for the $AuPd/TiO_2$ catalysts prepared by FSP. The alloy particles were more uniform than those prepared by co-deposition precipitation and co-impregnation methods [4]. The major drawback of the traditional preparations of supported AuPd catalyst is the lack of homogeneity in particle size, shape, and composition of AuPd catalysts [4].

The superior catalytic performance of Au–Pd nanoparticles compared to the individual Au and Pd (so-called the synergistic effect of AuPd alloy) is usually related to either ensemble or ligand modification [5]. The ensemble modification of Au-Pd system is mainly the diluting effect where Pd is diluted by Au [6–10]. As the surface ratio of Au–Pd increases, contiguous Pd ensembles disappear and Pd atoms are separated by Au forming isolated Pd ensembles [6,7]. This effect is shown to be responsible for the enhancement of activity and selectivity for certain reactions, e.g., vinyl acetate synthesis and direct H_2O_2 synthesis [11,12]. The ligand modification refers to a change in the local electronic structure due to charge transfer, orbital rehybridization, or other changes in electronic structure, which is responsible for the elimination of self-poisoning

* Corresponding author. Fax: +66 2218 6877.
E-mail address: joongjai.p@chula.ac.th (J. Panpranot).

http://dx.doi.org/10.1016/j.apcata.2015.09.012
0926-860X/

effect and the improvement in activity/selectivity, for examples, in hydrodesulfurization, CO oxidation, and acetylene trimerization [13–16].

The partial hydrogenation of unsaturated organic compounds for the synthesis of fine organic chemicals, e.g., selective hydrogenation of alkyne to the corresponding alkene is both of industrial and academic importance. Alkene products obtained via this reaction are useful in the synthesis of biological active compounds, the production of margarine, the lubricant industry, and the synthesis of important intermediates for fine chemical industries such as food (flavors), pharmaceutical (vitamins, sedatives), and cosmetics (fragrances) [17–19]. The selective hydrogenation of alkyne over monometallic Pd and bimetallic Pd–Au catalysts has been focused on both gas-phase and liquid-phase [1,4,20–25]. The dilution of Pd ensemble by Au atoms has shown to result in the improvement of hydrogenation activity [26,27]. A number of studies also reported the modification of activity and selectivity of supported Au–Pd catalysts due to electron transfer between Au and Pd [28–31]. For example, Chen and Lee [32] suggested that Pd could donate some electrons to Au, resulting in the hydrogen adsorption ability of Au, and as a consequence, the activity in the selective hydrogenation of *p*-chloronitrobenzene increased. Nevertheless, the degrees of AuPd alloying effect appeared to depend on several factors such as the molar ratio of Au to Pd, the preparation method, the particle morphology, the alloy particle size, and the metal-support interaction [24,25,33–35].

Despite the variety of supports being used for preparation of supported Au-Pd catalysts such as γ-Al_2O_3 [26,36], SiO_2 [29], SiO_2-Al_2O_3 [37], CeO_2 [38], carbon [39], and TiO_2 [4,25,36,40], only a few studies systematically reported the influence of support nature on the interaction of Au–Pd species and their corresponding catalytic behavior. Smolentseva et al. [38] showed that Pd–Au/Al_2O_3 exerted more pronounced interaction between gold and palladium species than Pd–Au/CeO_2 but the Pd–Au/CeO_2 manifested higher activity and selectivity in the selective oxidation of arabinose to arabinonic acid. The interaction of Au and Pd with reducible ceria coexisted with the mutual interaction between these metals. On the other hand, Kolli et al. [36] reported that the nature of supports between Al_2O_3 and TiO_2 had negligible effect on the composition of AuPd metal particles and did not participate in the selective hydrogenation of butadiene. In our recent study [40], the exertion of electronic modification by Au–Pd alloy was found to depend on the TiO_2 crystallite size in which the modification was more pronounced on the larger TiO_2 (15 nm) compared to the smaller one (9 nm), resulting in higher activity and lower selectivity in the selective hydrogenation of 1-heptyne.

High temperature reduction (i.e., at 500 °C) usually manifests the strong metal-support interaction (SMSI) of TiO_2 and group VIII transition metals (e.g., Pd, Pt, Ni, and Ir). The beneficial effect of SMSI on the catalyst performances has been reported for supported Pd/TiO_2 in the selective hydrogenation of acetylenic compounds [41–43]. However, the effect of reduction temperature on the characteristics and catalytic performances of AuPd alloy particles has not been investigated to much of a degree.

In the present work, the effect of reduction temperature on the catalytic performances of bimetallic Au-Pd/TiO_2 was investigated and compared to the monometallic Pd/TiO_2 in the liquid-phase selective hydrogenation of 1-heptyne under mild reaction conditions. Prior to the reaction tests, the catalysts were pretreated under hydrogen reduction temperature of 40 or 500 °C. The characteristics of catalysts were also investigated by X-ray diffraction (XRD), N_2 physisorption, temperature-programmed reduction (H_2-TPR), X-ray photoelectron spectroscopy (XPS), and transmission electron spectroscopy-energy dispersive X-ray spectroscopy (TEM-EDX).

2. Experimental

2.1. Catalyst preparation

The monometallic 1 wt.% Pd/TiO_2 and bimetallic 1 wt.% Au-1 wt.% Pd/TiO_2 catalysts were prepared by one-step FSP as described elsewhere [1,4]. Gold (III) chloride trihydrate (Sigma–Aldrich), palladium (II) acetylacetonate (Aldrich), and titanium (IV) butoxide (Aldrich) were chosen as Au, Pd, and TiO_2 precursors, respectively. The liquid precursor solution was prepared by dissolving all precursors into the mixture solution of xylene/acetonitrile (70/30 vol%) at total concentration of 0.5 M, then feeding into the flame reactor by using a syringe pump at a flow rate of 5 mL/min and dispersing with oxygen at a flow rate of 5 L/min to form the fine spray droplet after that. The pressure drop at the capillary tip was constantly adjusted at 1.5 bar by tuning the orifice gap area at the nozzle. To ignite the spray flame, oxygen and methane were provided as the supporting flame feed gases through a ring around the nozzle outlet at a flow rate of 3 and 1.5 L/min, respectively. The additional sheath oxygen was supplied through a sintered metal plate ring at flow rate of 25 L/min. A glass fiber filter with the aid of a vacuum pump was used to collect the product particles formed. The monometallic Pd/TiO_2 catalyst and TiO_2 support were also prepared by FSP method under similar conditions. The monometallic Pd/TiO_2 and bimetallic AuPd/TiO_2 catalysts were pretreated under hydrogen atmosphere (50 cm^3/min) at 40 and 500 °C for 2 h before being tested for catalytic performance. The monometallic Pd/TiO_2 and bimetallic AuPd/TiO_2 catalysts reduced at 40 and 500 °C are denoted as Pd/TiO_2 R40, Pd/TiO_2 R500, AuPd/TiO_2 R40, and AuPd/TiO_2 R500, respectively.

2.2. Catalyst characterization

The X-ray diffraction analysis was conducted on XRD D8 Advance of Bruker AXS with Ni-filter CuKα (λ = 1.54056 A°) radiation from 20° to 80° 2θ and step size of 0.020563 (step time = 88.5 s). The nitrogen physisorption technique was used to determine the BET specific surface area, pore volume, and pore diameter by using a Micromeritics ASAP 2020 automated system. The sample was degassed at 200 °C for 2 h (heating rate of 2.0 °C /min) under vacuum prior to N_2 adsorption analysis, which was carried out at liquid nitrogen temperature (−196 °C). XPS was performed using a Kratos Ultra DLD X-ray photoelectron spectrometer. The in situ high-energy XPS analysis was performed under reducing condition to ensure that the catalysts are in the active form. The C1s peak was used as reference at binding energy of 285.0 eV to calibrate for all XPS spectra. The TEM observations were performed in a JEOL JEM 2010 transmission electron microscope equipped with a LaB_6 electron beam source, a UHR polepiece (point resolution: 0.196 nm) and a Pentafet-Link Energy-Dispersive X-ray (EDX) spectrometer (and INCA software) from Oxford Instruments. The reducibility of catalyst as a function of temperature (TPR profile) was investigated by temperature programmed reduction technique using a MicromeriticsChemiSorb 2750 with ChemiSoftTPx software. Approximately 0.1 g of catalyst was pretreated under N_2 (25 mL/min) at 400 °C for 1 h before the TPR analysis in order to remove possible impurities contained in the samples. After cooling down to room temperature under N_2, the sample was exposed to mixture of 10% H_2 in Ar flowing at 25 mL/min with the temperature ramped of 10 °C/min from 35 °C to 700 °C. The temperature was held at 700 °C for 1 h and then cooled to room temperature. The actual amounts of Au and Pd were determined by the ICP-OES using the Optima 2100 DV spectrometer.

2.3. Catalytic reaction study

To test the performance of the catalysts, the liquid-phase hydrogenation of 1-heptyne under mild reaction conditions was carried out using approximately 5 mg of reduced catalyst dispersed in 10 cm^3 reactant mixture of 1-heptyne (Aldrich) in toluene (2%v/v). The reaction was performed in a 100 cm^3 stainless steel autoclave reactor (JASCO, Tokyo, Japan) at a pressure of 4 bar H_2 and at temperature of 30 °C for 5–120 min. After that, the liquid product was collected and analyzed by using gas chromatography equipped with a flame ionization detector (FID) and GS-alumina capillary column. The catalytic reaction tests were conducted under the absence of mass transfer/diffusion resistance. The highest stirring speed (1000 rpm) was used to eliminate the external mass transfer resistance and the effect due to pore diffusion was minimized by using small particle size catalysts. The catalysts were thoroughly grinded into powder form prior to the reaction tests.

3. Results and discussion

3.1. Catalyst characterization

The effect of reduction temperature on the TiO_2 crystallite size, the ratio of anatase to rutile phase, actual metal loadings, and the physical properties of the FSP-made catalysts was investigated by XRD, ICP-OES, and N_2 physisorption and the results are shown in Table 1. The crystallite sizes of anatase phase TiO_2 for both monometallic Pd/TiO_2 and bimetallic $AuPd/TiO_2$ catalysts did not change significantly with increasing reduction temperature from 40 °C to 500 °C (24–26 nm). However, the ratio of anatase to rutile phase composition decreased slightly with increasing reduction temperature, suggesting phase transformation of the TiO_2 from anatase to rutile under high reduction temperature. High reduction temperature weakened the Ti—O—Ti network and facilitated the Ti—O bond breaking, resulting in a structural rearrangement to the thermally stable rutile phase [44]. Compared to the monometallic ones, phase transformation of anatase to rutile TiO_2 on the bimetallic $AuPd/TiO_2$ catalysts was suppressed. For the bare TiO_2, phase transformation to rutile was also observed with a slightly higher ratio of anatase to rutile (decreased from 4.9 to 4.3 after reduction at high temperature) compared to the ones with Pd or AuPd addition during FSP synthesis (4.7). The role of metal dopant on phase transformation of TiO_2 has been reported and is usually based on the assumptions of substitutional and interstitial solid solubility [45]. The metal dopant in substitutional form may increase oxygen vacancy level and promote phase transformation (through increasing in lattice relaxation), while the interstitial form of metal dopant may enhance lattice constraint and inhibit phase transformation [45,46]. During FSP synthesis, in which the metal precursors containing Ti, Au, and Pd were fed into the reactor simultaneously, the role of Au and Pd dopants was based on the assumption of Ti^{4+} substitution, so the rutile phase transformation was facilitated. The results in this study are consistent to those reported previously by Paulauskas et al. [47] that %rutile phase TiO_2 increased in the metal-doped TiO_2 synthesized by FSP. Comparing between monometallic and bimetallic samples, the change of anatase to rutile ratio upon high temperature reduction was more pronounced on the monometallic catalysts. This is probably because the reduction of PdO occurred on the Pd/TiO_2 which may result in an increase in the number of oxygen vacancies and lattice relaxation so that rutile phase transformation was promoted. Whilst most of Pd was in the state of Pd-Au alloy in the in the bimetallic $AuPd/TiO_2$. The BET specific surface area, pore volume, and average pore diameter of both catalysts did not change significantly with increasing reduction temperature.

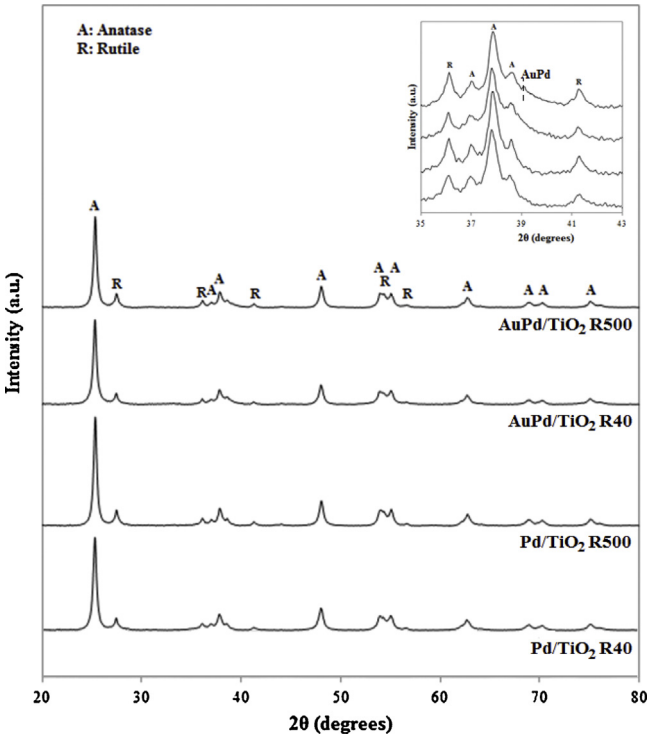

Fig. 1. XRD patterns over a scan range from 20° to 80° 2θ of (a) Pd/TiO_2 R40 (b) Pd/TiO_2 R500 (c) $AuPd/TiO_2$ R40 (d) $AuPd/TiO_2$ R500 catalysts (in-set: XRD patterns over a scan range from 35° to 45° 2θ of (a) Pd/TiO_2 R40 (b) Pd/TiO_2 R500 (c) $AuPd/TiO_2$ R40 (d) $AuPd/TiO_2$ R500 catalysts).

The XRD patterns of the bimetallic $AuPd/TiO_2$ and monometallic Pd/TiO_2 reduced at 40 °C and 500 °C are shown in Fig. 1. The characteristic XRD peaks for all the catalysts showed the presence of anatase and rutile TiO_2 phases, corresponding to the standard #JCPDS 84-1286 and #JCPDS 88-1175, respectively. The XRD peaks for Pd metal or PdO could not be observed for both catalysts due probably to the low Pd loading content and/or high dispersion of Pd nanoparticles on the TiO_2 supports. However, the XRD peaks corresponding to the (1 1 1) plane of AuPd alloy nanoparticles can be observed for the FSP-prepared bimetallic $AuPd/TiO_2$ catalysts as shown in Fig. 1. According to literature [48], AuPd alloy exhibited the XRD peak at 38.7° of (1 1 1) plane, while the mixture of separate Pd and Au exhibited two XRD peaks of Pd (1 1 1) plane at 39.8° and Au (1 1 1) plane at 38.2°, indicating the formation of an AuPd alloy for the former with an intermediate lattice parameter between that of Pd and Au and the presence of two different phases for the latter. The adding Au was considered to be helpful to protect Pd^0 from being oxidized into PdO [25].

The reducibility of catalyst samples was investigated by H_2-TPR and the results are shown in Fig. 2. According to the H_2-TPR results, the negative peaks at low temperature (~65 °C) observed for all the catalyst samples except the bare TiO_2 support which were attributed to the decomposition of Pd hydride (PdH_x) formed earlier with H_2. The Pd metal particles have the ability to absorb hydrogen within their structure to form Pd hydride at room temperature [49]. The decomposition of Pd hydride over supported Pd has been reported in the literature to occur in the temperature range of 323–373 K [50–53]. The absence of any detectable H_2 consumption signal (positive TPR peak) in advance of H_2 release (negative TPR peak) indicates a room temperature reduction [54]. There is a general agreement in the literature that H_2 uptake at room temperature corresponds to the reduction of supported and unsupported PdO at room temperature [55–57]. For the bimetallic Au-Pd catalysts, the peak area for Pd hydride decomposition was lower compared to

Table 1
TiO_2 crystallite size and ratio anatase to rutile phase based on the XRD results, actual metal loadings, and the N_2 physisorption properties.

Catalysts		Crystallite size of anatase TiO_2 (nm)	Ratio of anatase to rutile phase TiO_2[a]	Actual metal loadings[b]		N_2 physisorption results		
				Pd (wt.%)	Au (wt.%)	BET surface area (m^2/g)	Pore volume (cm^3/g)	Average pore diameter (nm)
Pd/TiO_2	R40	24	4.7 (82.3:17.7)	0.9	n/a	66	0.37	22
	R500	26	3.8 (79.4:20.6)	0.9	n/a	67	0.38	23
$AuPd/TiO_2$	R40	25	4.7 (82.4:17.6)	0.9	0.9	74	0.40	22
	R500	27	4.1 (80.3:19.7)	0.9	0.9	65	0.37	23

n/a: not available.
[a] Percentages of anatase and rutile TiO_2 phase compositions were determined according the method described in Ref. [105].
[b] Based on the ICP-OES results.

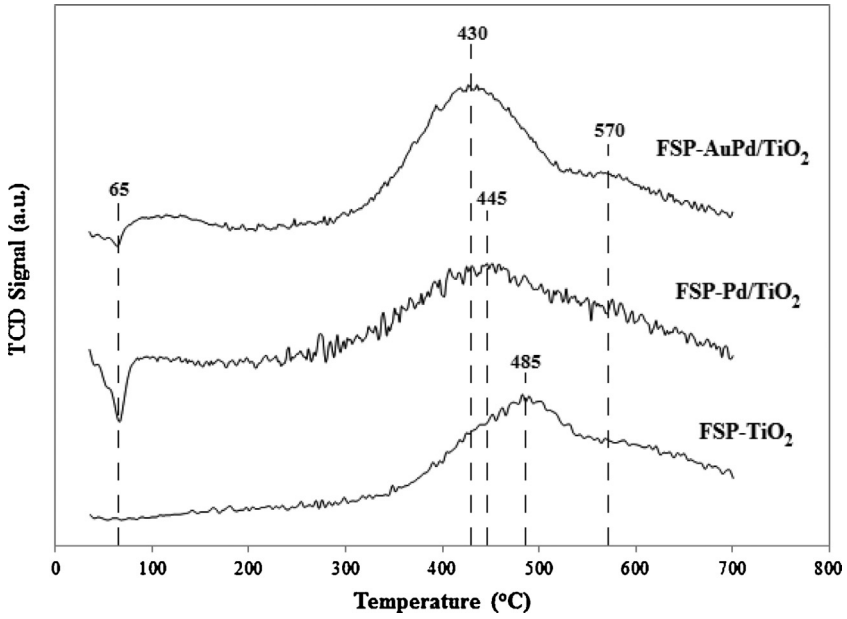

Fig. 2. H_2 temperature-programmed reduction profiles of TiO_2 support, Pd/TiO_2, and $AuPd/TiO_2$ catalysts.

the monometallic ones, suggesting a decrease in the Pd hydride species being formed and/or most of Pd species in the bimetallic $AuPd/TiO_2$ were incorporated as the AuPd alloy nanoparticles. This indicated that Pd hydride formation could be suppressed by the presence of AuPd alloy. Such an effect has also been reported by Krawczyk et al. [58] and Lingaiah et al. [50] when a second metal e.g., In and Fe was added to supported Pd catalysts. According to the literatures, the effect of hydride formation in supported Pd catalysts was found to be less pronounced than the effect of alloying with Ag [59,60]. Tew et al. also investigated the role of hydride in oxide-supported Pd nanoparticles for alkyne hydrogenation and showed that hydride species were not essential for complete hydrogenation to occur [61]. Furthermore, the Pd hydride should be decomposed already upon reduction at high temperature prior to the catalytic tests. Regarding the reduction of the AuPd alloy, a small broad peak between 90 and 120 °C was observed for the $AuPd/TiO_2$ and could be attributed to the reduction of Au_xPd_yO to Au_xPd_y alloy [62,63].

The TPR profiles of the TiO_2 supports indicate the partial reduction of the TiO_2 support itself at higher temperature. The reduction of Ti^{4+} to Ti^{3+} and Ti^{3+} to $Ti^{<3+}$ was observed at 485 °C and >520 °C, respectively. The partial reduction of TiO_2 has been reported to occur at $T \geq 500$ °C and was dependent on the TiO_2 structure [55,64,65]. Compared to the bare TiO_2 supports, the reduction peak of the TiO_2 shifted slightly towards lower temperature (shifted from 485 °C to 430 °C and 445 °C for $AuPd/TiO_2$ and Pd/TiO_2, respectively). The presence of noble metals (Pd or AuPd) facilitated the partial reduction of TiO_2 due to the hydrogen spillover from group VIII transition metals to the TiO_2 support [66]. The hydrogen molecules were dissociated on the noble metal particles (i.e., reduced Pd^0) into hydrogen atoms and spilled over onto the TiO_2 support and then partially reduced the TiO_2 to $TiO_{(2-x)}$ [67–69].

XPS analysis was used to determine the chemical composition and electronic structure of chemical species on the surface of the catalyst samples. The binding energies of Pd $3d_{5/2}$ and Au $4f_{7/2}$, are summarized in Table 2. The typical binding energy of Pd and Au was reported to be in the range of 335.0–335.4 eV [70] and 83.8–84.0 eV [71], respectively. For the monometallic Pd/TiO_2 catalysts, the binding energy for Pd $3d_{5/2}$ XPS moved from 337.3 eV to 334.6 eV after reduction at high temperature. For the bimetallic $AuPd/TiO_2$, both the Pd $3d_{5/2}$ and Au $4f_{7/2}$ peaks shifted towards lower binding energies, compared to Pd and Au metals, which may be attributed to Au–Pd alloy formation. The Pd $3d_{5/2}$ and Au $4f_{7/2}$ peaks for $AuPd/TiO_2$ R40 were observed at 334.8 eV and 82.7 eV, respectively. When reduced at higher temperature, the XPS peak of Pd $3d_{5/2}$ decreased further to 334.5 eV, due probably to more alloy formation. Typically a shift of the binding energies due to charge transfer from Pd to Au indicates an alloy formation [72]. For the Pd–Au system upon alloying, Au gains s, p electron and loses d electron whereas Pd loses s, p electrons but gains d electrons. Au is one of the most electronegative metallic elements, so upon alloying with Pd, a result of net charge transfer from Pd site to Au site is expected [6,73]. The negative shift of Pd 3d binding energy

Table 2
XPS and EDX results.

Catalysts		Binding energy (eV)		Atomic concentration		Atomic ratio			Atomic concentration (EDX)
		Pd 3d	Au 4f	Pd(%)	Au(%)	Pd/Ti	Au/Ti	(Pd+Au)/Ti	Pd/Au
Pd/TiO_2	R40	337.3	n/a	0.37	n/a	0.013	n/a	n/a	n/a
	R500	334.6	n/a	0.32	n/a	0.010	n/a	n/a	n/a
$AuPd/TiO_2$	R40	334.8	82.7	0.67	0.40	0.022	0.013	0.035	1.66
	R500	334.5	82.7	0.54	0.32	0.017	0.010	0.028	1.78

n/a: not available

compared to the monometallic Pd due to the gaining of d electrons upon AuPd alloying has been observed in several cases including unsupported Pd-Au alloys [72], Au_xPd_y/SiO_2 [13], and $AuPd/CeO_2$ [74]. Considering the electronic state of Pd 3d for Pd/TiO_2 R40, the binding energy appeared at 337.3 eV indicated to the PdO formation at surface. Although the TPR results revealed that reduction of PdO took place after reduction in H_2 at 40° for 2 h, re-oxidation of the Pd metal at the surface of the Pd/TiO_2 catalyst upon contacting with air was likely. According to the literatures [75], the small domains of Pd metal at the surface are easy to re-oxidize upon cooling to room temperature in air forming the surface oxide phase which can be seen by XPS while the bulk oxide was not detected by XRD or TEM. In addition, Melendez and Hoflund [76] reported that the smaller Pd particles are easier to oxidize and to form PdO layer than the larger Pd particles. Nevertheless, by reduction at 500 °C or alloying with Au, the Pd particles were found to be more resistant re-oxidation at the surface.

Elemental compositions at the catalyst surface (atomic%) are presented in Table 2. The ratios of Pd/Ti and (Au + Pd)/Ti decreased when the catalysts were reduced at 500 °C, due probably to the migration of TiO_x species onto the metals during high temperature reduction, or so-called the SMSI effect [69,77,78]. The decrease in Pd/Ti atomic ratio on the catalyst surface was observed by ca. 23% on both catalysts, suggesting that the SMSI effect occurred with a similar degree on the monometallic Pd/TiO_2 and bimetallic $AuPd/TiO_2$. It should be noted that the Au:Pd alloy composition of the $AuPd/TiO_2$, as determined by ICP, did not change with the reduction temperature (remained at 0.9 wt.% for both Au and Pd). Although little is known about the effect of H_2 reduction temperature on the surface composition of AuPd alloy, some previous studies have reported changes of AuPd alloy morphology upon heat treatment. For examples, Herzing et al. [79] reported a change from homogeneous alloy of the as-synthesized 2.5 wt.% Au-2.5 wt.% Pd/Al_2O_3 catalysts to Pd-rich shell/Au-rich core morphology after heat treatment (calcination) under air atmosphere. Moreover, the Pd/Au ratio at the surface increased with increasing heat treatment temperature from 200 °C to 400 °C, indicating Au depletion from the surface and Pd migration to the surface. However, the subsequent reduction treatment (H_2, 500 °C for 5 h) showed the inversion of core-shell morphology (the Pd-rich shell/Au-rich core morphology of the catalyst was changed into Pd-rich core/Au-rich shell). Edwards et al. [80], however, revealed that the Pd/Au ratio at the surface increased slightly from 1.0 to 1.4 with increasing temperature to 400 °C. In addition, treatment under O_2 and CO/O_2 was found to induce Pd segregation at the surface of the $AuPd/TiO_2$ nanoparticles (Au/Pd atomic ratio = 8) [81].

From the prediction of simple surface energetics, the surface free energies of Pd and Au are 2.043 J/m^2 and 1.626 J/m^2, respectively. Thus, Au would preferentially decorate the surface in order to minimize the surface free energy [82]. However, the nature and structure morphology of AuPd particles is dependent upon both heat treatment temperature and atmosphere. It appeared that preparation of the TiO_2 supported AuPd alloy by the single step FSP resulted in uniform AuPd particles with high thermal stability so that the composition of AuPd did not change upon high temperature reduction (500 °C).

TEM images of the monometallic Pd/TiO_2 and bimetallic $AuPd/TiO_2$ catalysts reduced at 40 and 500 °C are shown in Fig. 3 along with the particle size distribution in Fig. 4. The average metal particle size was determined from TEM images of approximately 500 particles. The $AuPd/TiO_2$ R40 catalysts exhibited uniform AuPd alloy nanoparticles distribution with average particle size of 2–5 nm. After reduction at high temperature, a slight increase in the average size is observed from 3.8 nm to 4.5 nm. The geometric standard deviation of the $AuPd/TiO_2$ R40 and the $AuPd/TiO_2$ R500 were calculated to be 1.27 and 1.50, respectively. For the monometallic Pd/TiO_2 catalysts, the Pd particles in the TEM images of the Pd/TiO_2 R40 and Pd/TiO_2 R500 catalysts were quite difficult to visualize but we can determine their sizes to be in the range of 2–3 nm whatever the reduction temperature. This difficulty in detecting Pd nanoparticles may be due to the fact that Pd is "lighter" than Au (and of course bimetallic AuPd) and so the arising contrasts from very small particles are weaker; also we have to take into account the nature of the support since titania may render the detection of very small nanoparticle contrasts rather difficult due to electron absorption which is not observed for other oxide supports such as silica and alumina [83–85] or non-oxide supports such as nitrides [85–87] or carbonaceous materials [88–91]. As it was mentioned in the experimental section, the TEM instrument used to perform imaging and EDX is equipped with a LaB_6 thermoionic gun. With such an electron source it is difficult to work with probes below 5–10 nm in diameter since the amount of current is rather low and, as a result, spectra acquisition in EDX is rather long and inconsistent with particle evolution under the electron beam (diffusion, damage, ...), especially on small bimetallic nanoparticles (<5 nm). Taking into account previous studies on supported bimetallic nanoparticles [84,92,93] and in order to limit damage or any other evolution under the electron beam to negligible levels we have thus used a 10 nm electron probe to analyze small individual particles and a slightly decondensed 25 nm electron probe to analyze small groups of particles (2–5). To analyze large regions (several μm^2) we used a (largely) decondensed electron probe. EDX results presented in Fig. 5 clearly show that the nanoparticles were bimetallic for both $AuPd/TiO_2$ R40 and $AuPd/TiO_2$ R500 catalysts. Composition determined from large regions show that both samples are (35 ± 3)% at Au and (65 ± 3)% at Pd which in very good agreement with value expected from ICP (35% at Au) and very close to the XPS measurements (37% at Au for both samples) which are also performed over large regions. This reveals indeed that the entirety of the bimetallic nanoparticles were analyzed both by EDX (since the electron beam probes all the particles) and XPS (since it is sensitive to a thickness of around 5–10 nm and the nanoparticles are below 5 nm for a very large majority of them). The EDX analysis of individual nanoparticles (see Fig. 5) reveals that the nanoparticles in $AuPd/TiO_2$ R40 were less homogeneous in composition than those in $AuPd/TiO_2$ R500. From the measurements, the Au composition of the $AuPd/TiO_2$ R40 was 37.7% at. with a standard deviation ±9.6 whereas that of the $AuPd/TiO_2$ R500 was 36.3% at. with a standard deviation ±3.6. In other word, the higher temperature

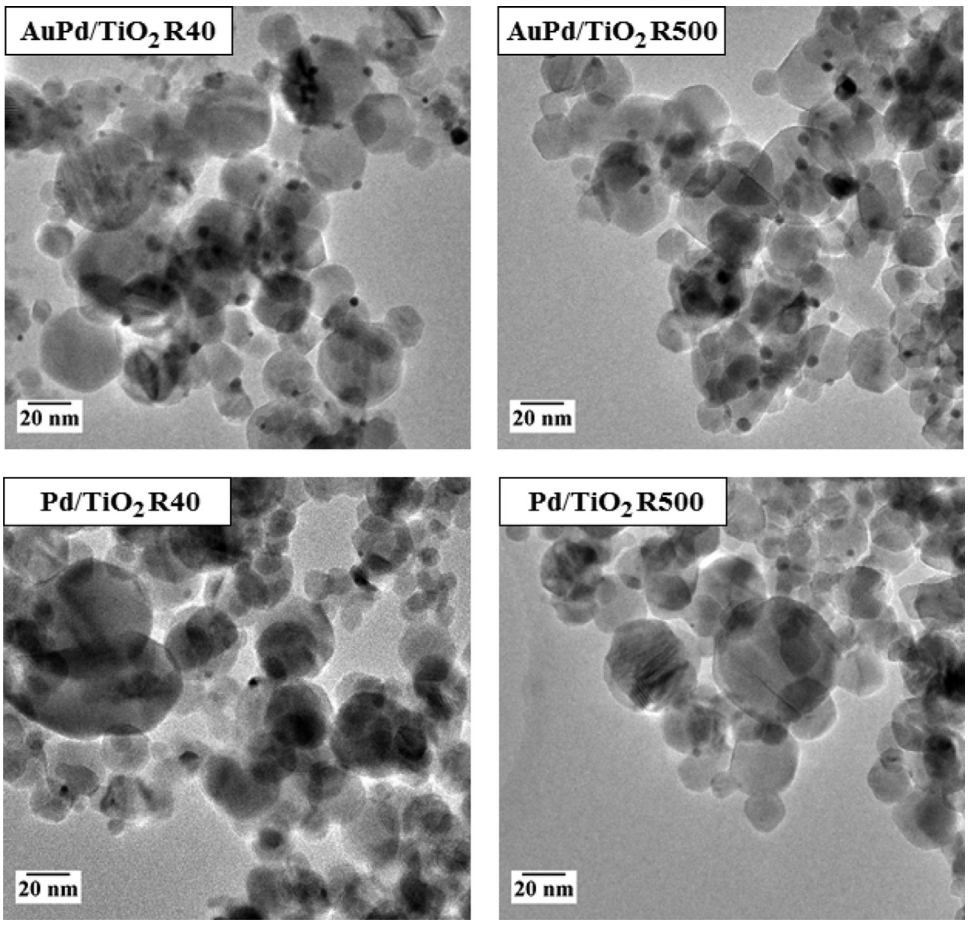

Fig. 3. TEM images of (a) AuPd/TiO_2 R40 (b) AuPd/TiO_2 R500 (c) Pd/TiO_2 R40 (d) Pd/TiO_2 R500.

reduction tends to homogenize the composition of the individual nanoparticles. One can thus obtain collections of supported bimetallic nanoparticles rather homogeneous in composition and comparable to what can be achieved by physical methods as, for instance, cluster deposition by laser ablation in vacuum [92,94] and liquids [93]. The FSP method has the advantage over the physical methods that it is easier to upscale for industrial applications. From the EDX results, the ratio of Pd/Au (atomic%) for bimetallic AuPd/TiO_2 as shown in Table 2. The ratios of Pd/Au for AuPd/TiO_2 were not significantly changed with increasing reduction temperature from 40 °C to 500 °C. This result corresponds to the Pd/Au composition on surface from the XPS results.

3.2. Reaction study in 1-heptyne hydrogenation

The catalytic performances of the FSP-made Pd/TiO_2 and AuPd/TiO_2 catalysts were evaluated in the selective liquid phase hydrogenation of 1-heptyne under mild conditions. The conversion of 1-heptyne, the selectivity to 1-heptene, and the yield of 1-heptene as a function of time for the catalysts reduced at 40 and 500 °C are presented in Fig. 6(a)–(c), respectively. The products from the reactions were 1-heptene and heptane, no other by-products were detected. The initial reaction rates were calculated at 10 min reaction time and the results are shown in Table 3. The order of the catalytic activity for 1-heptyne hydrogenation was as follows: AuPd/TiO_2 R40 > AuPd/TiO_2 R500 > Pd/TiO_2 R500 > Pd/TiO_2 R40. Within 60 min of the reaction time, complete conversion of 1-heptyne was obtained for all the FSP-made catalysts. The bimetallic AuPd/TiO_2 catalysts showed higher catalytic activity than the monometallic Pd/TiO_2, regardless of the reduction temperature.

Table 3
The reaction rates obtained at 10 min reaction time of the different catalysts.

Catalysts	Reaction rate (μmol s^{-1} g cat.$^{-1}$)
Pd/TiO_2 R40	170
Pd/TiO_2 R500	211
AuPd/TiO_2 R40	245
AuPd/TiO_2 R500	223

Error of measurements was ±3%.

The results are consistent with previous works where addition of Au as a second metal to form Au–Pd alloy improved the catalytic activity of Pd/TiO_2 in the selective hydrogenation of 1-heptyne [4,25,40]. According to literature [32,95,96], a small charge transfer from Pd to Au resulted in activated Au which could adsorb hydrogen. Schimpf et al. [96] reported that electron transfer to Au would result in the Au being enriched in valence electron density. Then a partial transfer of electron density to the π^* orbital of the unsaturated bond is facilitated and the interaction of the active sites with the functional group is altered.

However, the effect of reduction temperature on the catalyst performances was different between the Pd/TiO_2 and AuPd/TiO_2 catalysts. The activity of the Pd/TiO_2 increased when reduced at 500 °C due to complete reduction of PdO to metallic Pd^0 as revealed by the XPS results, despite the lower Pd/Ti ratio on the Pd/TiO_2 R500 catalyst. On the other hand, the bimetallic AuPd/TiO_2 R500 exhibited lower activity than the ones reduced at 40 °C. Because there were no significant changes in the particle size, the morphology, and alloy composition, the lower catalyst activity of the AuPd/TiO_2 R500 was attributed to the lower amount of the metals

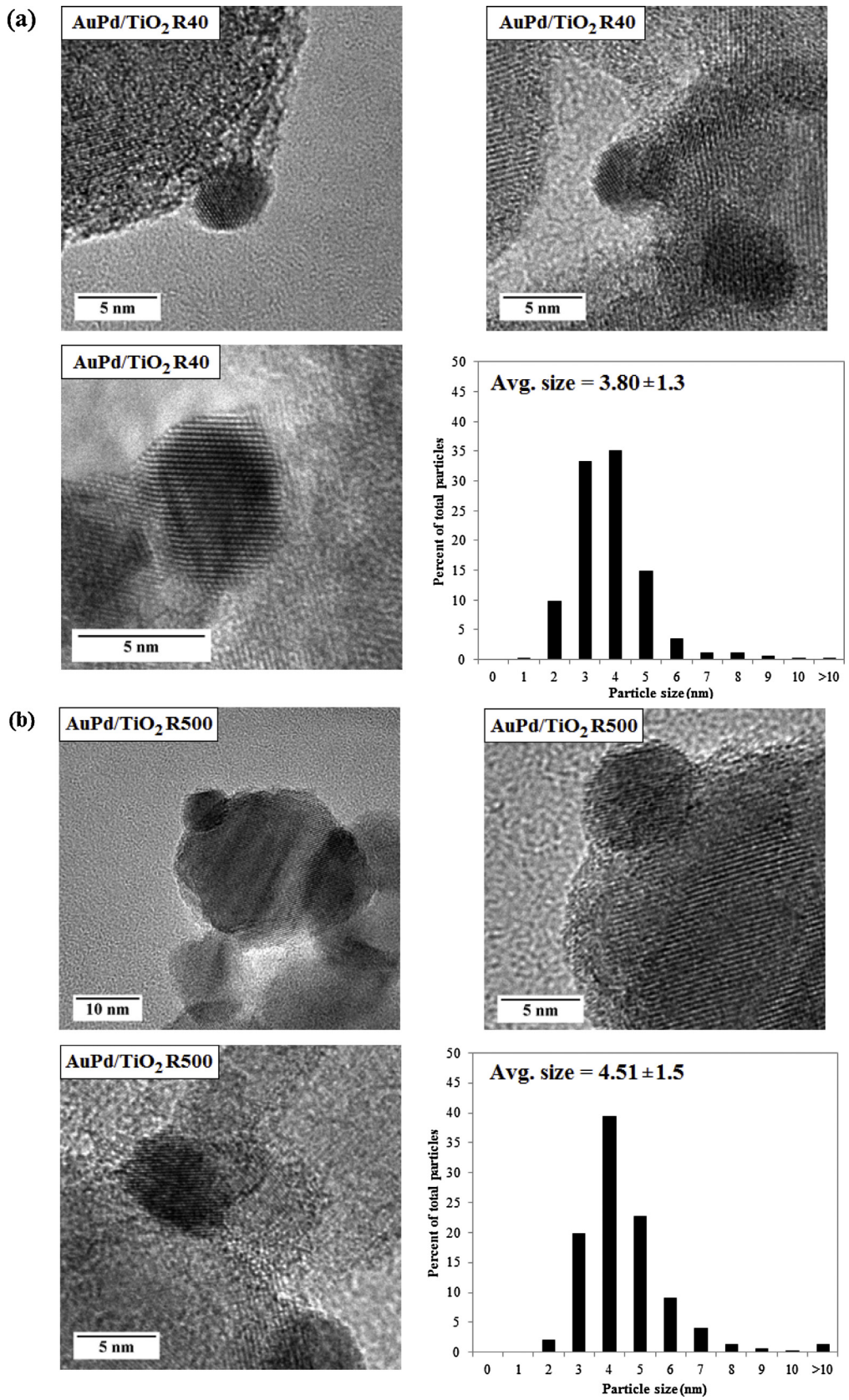

Fig. 4. HR-TEM images and particle size distribution of the bimetallic AuPd/TiO_2 catalysts reduced at 40 (a) and 500 °C (b).

on the surface (Au + Pd)/Ti upon high temperature reduction. The effect of high reduction temperature on the decrease of catalytic activity of alloying bimetallic particles has been reported for other catalyst systems such as Pt-Ge/Al_2O_3 and Pt-Sn/Al_2O_3 in hydrogenation/dehydrogenation reactions [97]. The catalytic activity of bimetallic Pt-Sn and Pt-Ge catalysts reduced at high tempera-

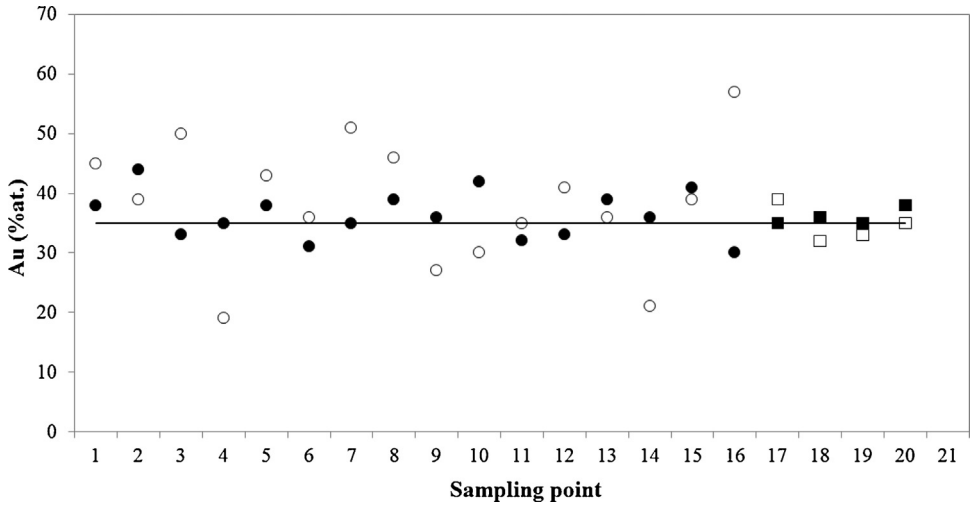

Fig. 5. Amount of Au (%at) in the bimetallic nanoparticles measured by EDX for AuPd/TiO_2 R40 (open circles and squares) and AuPd/TiO_2 R500 (black circles and squares). Measurements were made on individual nanoparticles or small groups (3–5) nanoparticles (circles) and on large regions (squares). The straight grey line indicates the nominal composition determined by ICP.

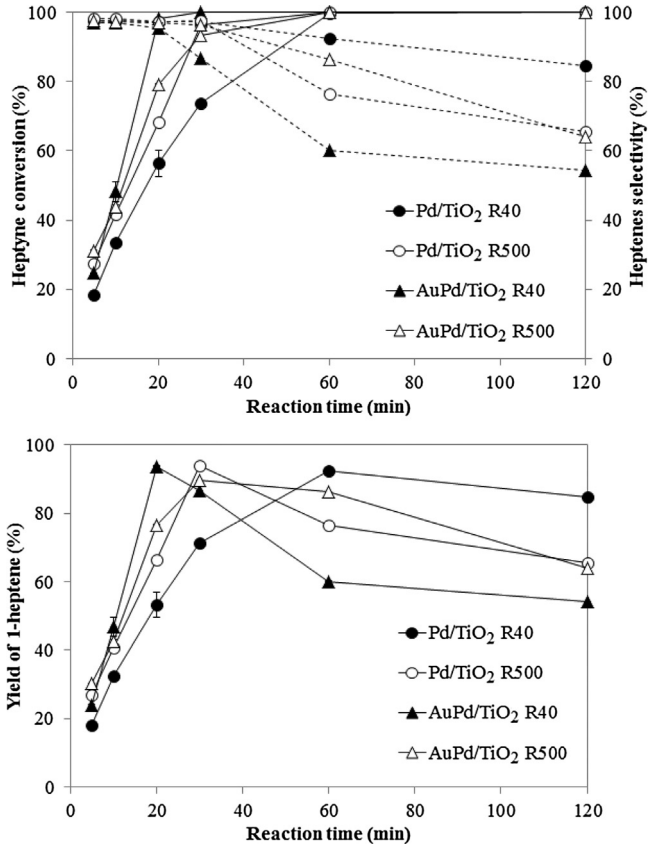

Fig. 6. Conversion of heptyne (solid line) and selectivity to 1-heptene (dash line) (a) and yield of 1-heptene (b) of the monometallic Pd/TiO_2 and bimetallic AuPd/TiO_2 catalysts reduced at 40 and 500 °C (error margin for the reported rates was 0–2%).

ture (500 °C) decreased drastically compared to bimetallic catalysts reduced at lower temperature (300 °C) and monometallic Pt catalyst. The temperature of hydrogen reduction treatment plays a crucial factor governing the hydrogenation activity not only for the bimetallic AuPd alloy nanoparticles, but also for the bimetallic Au core-Pd shell nanoparticles [98].

The selectivity to 1-heptene for all the FSP-made catalysts during the 30 min reaction time were nearly 100% except that of AuPd/TiO_2 R40 (the selectivity of 1-heptene 87%). Comparing at the same level of conversion (~99%), the selectivity to 1-heptene was found in the following order: AuPd/TiO_2 R40 > Pd/TiO_2 R40 > AuPd/TiO_2 R500 > Pd/TiO_2 R500 catalysts. Prolonging the reaction time to 120 min, the selectivity to 1-heptene for the Pd/TiO_2 R40, Pd/TiO_2 R500, and AuPd/TiO_2 R40 catalysts decreased to 85, 66, and 54%, respectively. Reduction at 500 °C resulted in a significant increase in selectivity of 1-heptene for the AuPd/TiO_2 R500 to 64% after 120 min reaction time.

Typically, TiO_2 manifests the SMSI effect with group VIII transition metals after high temperature reduction, resulting in the formation of Pd-TiO_x species which enhance the alkene selectivity in many alkyne hydrogenation reactions [99–101]. However, it should be noted that most of the catalysts reported to have such effects were prepared by conventional methods such as impregnation or deposition-precipitation of metal precursors on the TiO_2 supports. The results in this study showed that the SMSI effect may be less pronounced on the monometallic Pd/TiO_2 catalysts. Although there might be some migration of TiO_x species on the Pd surface of the Pd/TiO_2 R500, the changes of surface species from PdO to metallic Pd^0 showed grater effect on the catalyst performances so that the catalyst exhibited lower selectivity of 1-heptene compared to the one reduced at 40 °C with higher hydrogenation activity. On the other hand, for the bimetallic AuPd/TiO_2 in which the metal particles were already in the form of AuPd alloy in the as-prepared catalysts, reduction at 500 °C can improve the selectivity of 1-heptene from 54 to 64% after complete 1-heptyne conversion (prolonging reaction time to 120 min). According to the TPR results, the reduction of TiO_2 was also easier on the bimetallic AuPd/TiO_2 than on the monometallic Pd/TiO_2. Comparing the yield of 1-heptene as a function of reaction time for the various catalysts, the highest yield of 1-heptene (~93%) was obtained over the AuPd/TiO_2 R40 in the shortest reaction time (20 min) while high temperature reduction was required for the monometallic Pd/TiO_2 to exhibit similar level of 1-heptene yield at longer reaction time. The reaction results of the liquid phase 1-heptyne hydrogenation over supported Pd-based catalysts in this study are also compared to those reported in the literature as summarized in Table 4. The catalytic activity of the commercial Lindlar catalyst has been reported to be very low (conversion 5–45% for reaction time up to 150 min) [102]. The catalyst performances of Pd-based catalysts for the selective hydrogenation of 1-heptyne to 1-heptene were improved by the addition of a second metal such as W, Ni, and

Table 4
Comparison of the catalytic activity of supported Pd catalysts in the liquid-phase hydrogenation of 1-heptyne under mild conditions.

Catalysts	Preparation	Reaction conditions	Time (min)	Conversion (%)	Selectivity (%)	Yield (%)	Ref.
Pd/TiO_2	FSP	303 K, 4 bar	10	33	97	32	This study
R40			60	100	93	93	
Pd/TiO_2			10	42	98	41	
R500			30	96	98	94	
			60	100	76	76	
$AuPd/TiO_2$			10	48	97	47	
R40			20	98	95	93	
$AuPd/TiO_2$			10	44	97	43	
R500			30	93	96	89	
			60	100	86	86	
0.4%Pd-2.4%W/γ-Al_2O_3 reduced 120 °C	IMP	303 K,	30	18	98	18	[103]
		150 kPa	180	100	98	98	
0.4%Pd/Al_2O_3	IMP	303 K,	30	10	95	9.5	[102]
		150 kPa	150	18	98	18	
0.4%Pd-			30	13	96	12	
1%Ni/Al_2O_3			150	30	98	29	
Lindlar	Commercial		30	5	88	4	
			150	45	81	36	
$[PdCl_2(NH_2(CH_2)_{12}CH_3)_2]/\text{ɤ-}Al_2O_3$	IMP	303 K, 150 kPa	n/a	90	63	57	[106]
0.5%Pd-	IMP/DP	303 K, 1 bar	10	73	96	70	[25]
1%Au/TiO_2			30	100	55	55	
1%Pd/TiO_2	FSP	303 K, 1 bar	5	80	94	75	[1]
			40	100	90	90	
1%Pd/SiO_2	FSP	303 K, 105 kPa	5	43	92	40	[104]
			40	100	62	62	

FSP: flame spray pyrolysis, IMP: impregnation, DP: deposition.

Au [25,102,103]. Interestingly, the presence of Au and W on the Pd-based catalysts demonstrated remarkably high conversion and high selectivity [25,103]. Furthermore, TiO_2 supported monometallic Pd and bimetallic AuPd catalysts were synthesized in one-step by the FSP method and compared to those obtained by the conventional impregnation technique [1,4,104]. The catalytic performances of the FSP-made $AuPd/TiO_2$ catalysts in terms of 1-heptene yield are at state-of-the art (1-heptene yield ~93% at reduction temperature of 40 °C, 20 min reaction time). The yield of 1-heptene that has been reported over the other non-FSP made Pd-based catalysts was typically lower in the range of 4-75%. There was only one exceptional case of the 0.4%Pd-2.4%W/γ-Al_2O_3 reduced at 120 °C that 98% yield of 1-heptene was obtained at 303 K and 150 kPa after 3 h reaction time [103].

4. Conclusions

The reduction temperature strongly affected the catalytic performances of the FSP-synthesized TiO_2 supported monometallic Pd and bimetallic AuPd catalysts in the selective hydrogenation of 1-heptyne. For the Pd/TiO_2, reduction at 500 °C resulted in the complete reduction of PdO on the catalyst surface, leading to an improvement in hydrogenation activity and 1-heptene yield. On the other hand, the $AuPd/TiO_2$ R40 exhibited higher reaction rate and higher yield of 1-heptene than the $AuPd/TiO_2$ R500 under similar reaction conditions used. Based on the XPS and TEM-EDX results, there were no significant changes in the alloy particle size and the composition of Au:Pd alloy. Therefore, the lower catalytic activity was correlated to the lower active metal (Pd + Au)/Ti on the catalyst surface. The highest yield of 1-heptene (~93%) was obtained over the bimetallic FSP-$AuPd/TiO_2$ reduced at 40 °C in 20 min reaction time.

Acknowledgements

We gratefully thank the Dusadeepipat scholarship from Chulalongkorn University for B.P. and the Grant for International Research Integration: Chula Research Scholar, Ratchadaphiseksomphot Endowment Fund. The authors also acknowledge support from the National Research Council of Thailand (NRCT) under PHC SIAM no. 29626VJ.

References

[1] O. Mekasuwandumrong, S. Phothakwanpracha, B. Jongsomjit, A. Shotipruk, J. Panpranot, Catal. Lett. 136 (2010) 164–170.
[2] O. Mekasuwandumrong, S. Phothakwanpracha, B. Jongsomjit, A. Shotipruk, J. Panpranot, Powder Technol. 210 (2011) 328–331.
[3] L. Mädler, W.J. Stark, S.E. Pratsinis, J. Mater. Res. 18 (2003) 115–120.
[4] B. Pongthawornsakun, S.-i. Fujita, M. Arai, O. Mekasuwandumrong, J. Panpranot, Appl. Catal. A: Gen. 467 (2013) 132–141.
[5] V. Polshettiwar, T. Asefa, Nanocatalysis Synthesis and Applications, John Wiley & Sons, Inc., New Jersey, 2013.
[6] F. Gao, D.W. Goodman, Chem. Soc. Rev. 41 (2012) 8009–8020.
[7] J.-B. Chang, C.-H. Liu, J. Liu, Y.-Y. Zhou, X. Gao, S.-D. Wang, Nano-Micro Lett. 7 (2015) 307–315.
[8] C.-H. Cui, J.-W. Yu, H.-H. Li, M.-R. Gao, H.-W. Liang, S.-H. Yu, ACS Nano. 5 (2011) 4211–4218.
[9] P. Liu, J.K. Norskov, Phys. Chem. Chem. Phys. 3 (2001) 3814–3818.
[10] V. Ponec, Applied Catalysis A: Gen. 222 (2001) 31–45.
[11] D. Kumar, M.S. Chen, D.W. Goodman, Catal. Today 123 (2007) 77–85.
[12] H.-f. Yang, P.-y. Xie, H.-y. Yu, X.-n. Li, J.-g. Wang, Phys. Chem. Chem. Phys. 14 (16) (2012) 654–16659.
[13] A.M. Venezia, V. La Parola, G. Deganello, B. Pawelec, J.L.G. Fierro, J. Catal. 215 (2003) 317–325.
[14] F. Gao, Y. Wang, D.W. Goodman, J. Phys. Chem. C 113 (2009) 14993–15000.
[15] T. Ward, L. Delannoy, R. Hahn, S. Kendell, C.J. Pursell, C. Louis, B.D. Chandler, ACS Catal. 3 (2013) 2644–2653.
[16] R.M. Ormerod, C.J. Baddeley, R.M. Lambert, Surf. Sci. 259 (1991) L709–L713.
[17] M. Al-Herz, M.J.H. Simmons, J. Wood, Ind. Eng. Chem. Res. 51 (2012) 8815–8825.
[18] J.G. Ulan, W.F. Maier, D.A. Smith, J. Organ. Chem. 52 (1987) 3132–3142.
[19] P.C. L'Argentière, M.E. Quiroga, D.A. Liprandi, E.A. Cagnola, M.C. Román-Martínez, J.A. Díaz-Auñón, C. Salinas-Martínez de Lecea, Catal. Lett. 87 (2003) 97–101.
[20] D. Teschner, E. Vass, M. Hävecker, S. Zafeiratos, P. Schnörch, H. Sauer, A. Knop-Gericke, R. Schlögl, M. Chamam, A. Wootsch, A.S. Canning, J.J. Gamman, S.D. Jackson, J. McGregor, L.F. Gladden, J. Catal. 242 (2006) 26–37.
[21] D. Lamey, I. Prokopyeva, F. Cárdenas-Lizana, L. Kiwi-Minsker, Catal. Today 235 (2014) 79–89.
[22] W.-J. Kim, S.H. Moon, Catal. Today 185 (2012) 2–16.
[23] A. Sarkany, P. Hargittai, A. Horvath, Top Catal. 46 (2007) 121–128.
[24] T.V. Choudhary, C. Sivadinarayana, A.K. Datye, D. Kumar, D.W. Goodman, Catal. Lett. 86 (2003) 1–8.
[25] P. Kittisakmontree, B. Pongthawornsakun, H. Yoshida, S.I. Fujita, M. Arai, J. Panpranot, J. Catal. 297 (2013) 155–164.
[26] B. Pawelec, A.M. Venezia, V. La Parola, E. Cano-Serrano, J.M. Campos-Martin, J.L.G. Fierro, Appl. Surf. Sci. 242 (2005) 380–391.

[27] T. Redjala, H. Remita, G. Apostolescu, M. Mostafavi, C. Thomazeau, D. Uzio, Oil Gas Sci. Technol. Rev. IFP 61 (2006) 789–797.
[28] B. Pawelec, E. Cano-Serrano, J.M. Campos-Martin, R.M. Navarro, S. Thomas, J.L.G. Fierro, Appl. Catal. A: Gen. 275 (2004) 127–139.
[29] X. Yang, D. Chen, S. Liao, H. Song, Y. Li, Z. Fu, Y. Su, J. Catal. 291 (2012) 36–43.
[30] R. Liu, Y. Yu, K. Yoshida, G. Li, H. Jiang, M. Zhang, F. Zhao, S.-i. Fujita, M. Arai, J. Catal. 269 (2010) 191–200.
[31] D.I. Enache, D. Barker, J.K. Edwards, S.H. Taylor, D.W. Knight, A.F. Carley, G.J. Hutchings, Catal. Today 122 (2007) 407–411.
[32] Y. Chen, D. Lee, Mod. Res. Catal. 2 (2013) 25–34.
[33] P.J. Miedziak, Q. He, J.K. Edwards, S.H. Taylor, D.W. Knight, B. Tarbit, C.J. Kiely, G.J. Hutchings, Catal. Today 163 (2011) 47–54.
[34] P. Miedziak, M. Sankar, N. Dimitratos, J.A. Lopez-Sanchez, A.F. Carley, D.W. Knight, S.H. Taylor, C.J. Kiely, G.J. Hutchings, Catal. Today 164 (2011) 315–319.
[35] N. Dimitratos, J. Lopez-Sanchez, D. Lennon, F. Porta, L. Prati, A. Villa, Catal. Lett. 108 (2006) 147–153.
[36] N.E. Kolli, L. Delannoy, C. Louis, J. Catal. 297 (2013) 79–92.
[37] A.M. Venezia, V.L. Parola, B. Pawelec, J.L.G. Fierro, Appl. Catal. A: Gen. 264 (2004) 43–51.
[38] E. Smolentseva, B.T. Kusema, S. Beloshapkin, M. Estrada, E. Vargas, D.Y. Murzin, F. Castillon, S. Fuentes, A. Simakov, Appl. Catal. A: Gen. 392 (2011) 69–79.
[39] A. Villa, N. Janjic, P. Spontoni, D. Wang, D.S. Su, L. Prati, Appl. Catal. A: Gen. 364 (2009) 221–228.
[40] P. Kittisakmontree, H. Yoshida, S.-i. Fujita, M. Arai, J. Panpranot, Catal. Commun. 58 (2015) 70–75.
[41] J. Panpranot, K. Kontapakdee, P. Praserthdam, Appl. Catal. A: Gen. 314 (2006) 128–133.
[42] Y. Li, B. Xu, Y. Fan, N. Feng, A. Qiu, J.M.J. He, H. Yang, Y. Chen, J. Mol. Catal. A: Chem. 216 (2004) 107–114.
[43] P.S. Kumbhar, Appl. Catal. A: Gen. 96 (1993) 241–252.
[44] V. Etacheri, M.K. Seery, S.J. Hinder, S.C. Pillai, Adv. Funct. Mater. 21 (2011) 3744–3752.
[45] D.H. Hanaor, C. Sorrell, J. Mater. Sci. 46 (2011) 855–874.
[46] D.A.H. Hanaor, G. Triani, C.C. Sorrell, Surf. Coat. Technol. 205 (2011) 3658–3664.
[47] I.E. Paulauskas, D.R. Modeshia, T.T. Ali, E.H. El-Mossalamy, A.Y. Obaid, S.N. Basahel, A.A. Al-Ghamdi, F.K. Sartain, Platinum Met. Rev. 57 (2013) 32–43.
[48] J.-S. Lim, S.-M. Kim, S.-Y. Lee, E.A. Stach, J.N. Culver, M.T. Harris, J. Nanomater. 2010 (2010) 1–6.
[49] J. Panpranot, O. Tangjitwattakorn, P. Praserthdam, J.G. Goodwin Jr, Appl. Catal. A: Gen. 292 (2005) 322–327.
[50] N. Lingaiah, P.S. Sai Prasad, P. Kanta Rao, F.J. Berry, L.E. Smart, Catal. Commun. 3 (2002) 391–397.
[51] M. Bonarowska, B. Burda, W. Juszczyk, J. Pielaszek, Z. Kowalczyk, Z. Karpiński, Appl. Catal. B: Environ. 35 (2001) 13–20.
[52] N.K. Nag, J. Phys. Chem. B 105 (2001) 5945–5949.
[53] L.M. Gómez-Sainero, X.L. Seoane, J.L.G. Fierro, A. Arcoya, J. Catal. 209 (2002) 279–288.
[54] C. Amorim, X. Wang, M.A. Keane, Chin. J. Catal. 32 (2011) 746–755.
[55] H. Zhu, Z. Qin, W. Shan, W. Shen, J. Wang, Journal of Catalysis. 225 (2004) 267–277.
[56] C.-B. Wang, H.-K. Lin, C.-M. Ho, J. Mol. Catal. A: Chem. 180 (2002) 285–291.
[57] G.M. Tonetto, D.E. Damiani, J. Mol. Catal. A: Chem. 202 (2003) 289–303.
[58] N. Krawczyk, I. Witonska, A. Krolak, M. Frajtak, S. Karski, Rev. Roum. Chim. 56 (2011) 595–600.
[59] A.J. McCue, J.A. Anderson, Front. Chem. Sci. Eng. 9 (2015) 142–153.
[60] A. Hazra, S.K. Hazra, D. Dutta, C.K. Sarkar, S. Basu, Front. Sens. 1 (2013) 17–26.
[61] M.W. Tew, M. Janousch, T. Huthwelker, J.A. van Bokhoven, J. Catal. 283 (2011) 45–54.
[62] L. Chen, S. Wang, C. Chen, N. Zhang, Transition Met. Chem. 36 (2011) 387–393.
[63] Q.-b. Chen, L.-t. Luo, X. Yang, Ind. J. Chem. 47A (2008) 1317–1322.
[64] F. Wyrwalski, J.-M. Giraudon, J.-F. Lamonier, Catal. Lett. 137 (2010) 141–149.
[65] M. Bowker, Curr. Opin. Solid State Mater Sci. 10 (2006) 153–162.
[66] C. Zhang, H. He, K.-i. Tanaka, Appl. Catal. B: Environ. 65 (2006) 37–43.
[67] J. Hong, W. Chu, M. Chen, X. Wang, T. Zhang, Catal. Commun. 8 (2007) 593–597.
[68] Y. Zhu, D. Liu, M. Meng, Chem. Commun. 50 (2014) 6049–6051.
[69] Z. Paaíl, P.G. Menon, Hydrogen Effects in Catalysis: Fundamentals and Practical Applications, M. Dekker, New York, 1988.
[70] M. Jin, J.-N. Park, J.K. Shon, J.H. Kim, Z. Li, Y.-K. Park, J.M. Kim, Catal. Today 185 (2012) 183–190.
[71] A. Beck, A. Horváth, Z. Schay, G. Stefler, Z. Koppány, I. Sajó, O. Geszti, L. Guczi, Top Catal. 44 (2007) 115–121.
[72] P.A.P. Nascente, S.G.C. de Castro, R. Landers, G.G. Kleiman, Phys. Rev. B 43 (1991) 4659–4666.
[73] Y.-S. Lee, Y. Jeon, Y.-D. Chung, K.-Y. Lim, C-N, S.-J.O.H. Whang, J. Korean Phys. Soc. 37 (2000) 451–455.
[74] Z. Zhang, Y. Wang, X. Li, W.-L. Dai, Chin. J. Catal. 35 (2014) 1846–1853.
[75] A.K. Datye, J. Bravo, T.R. Nelson, P. Atanasova, M. Lyubovsky, L. Pfefferle, Appl. Catal. A: Gen. 198 (2000) 179–196.
[76] O. Melendez, G.B. Hoflund, 18th North American Catalysis Society Meeting, Cancun, Mexico, 2009.
[77] P.L. Gai, E.D. Boyes, Electron microscopy in heterogeneous catalysis, Institute of Physics Publishing, London, 2003.
[78] R.L. Augustine, Heterogeneous Catalysis for the Synthetic Chemist, M. Dekker, New york, 1996.
[79] A.A. Herzing, A.F. Carley, J.K. Edwards, G.J. Hutchings, C.J. Kiely, Chem. Mater. 20 (2008) 1492–1501.
[80] J.K. Edwards, J. Pritchard, M. Piccinini, G. Shaw, Q. He, A.F. Carley, C.J. Kiely, G.J. Hutchings, J. Catal. 292 (2012) 227–238.
[81] L. Delannoy, S. Giorgio, J.G. Mattei, C.R. Henry, N. El Kolli, C. Méthivier, C. Louis, ChemCatChem 5 (2013) 2707–2716.
[82] C.W. Yi, K. Luo, T. Wei, D.W. Goodman, J. Phys. Chem. B 109 (2005) 18535–18540.
[83] A. Goguet, M. Aouine, F.J. Cadete Santos Aires, A. De Mallmann, D. Schweich, J.P. Candy, J. Catal. 209 (2002) 135–144.
[84] K. Pattamakomsan, E. Ehret, F. Morfin, P. Gélin, Y. Jugnet, S. Prakash, J.C. Bertolini, J. Panpranot, F.J.C.S. Aires, Catal. Today 164 (2011) 28–33.
[85] G. Garcia Cervantes, F.J. Cadete Santos Aires, J.C. Bertolini, J. Catal. 214 (2003) 26–32.
[86] I. Kurzina, F.J. Cadete Santos Aires, G. Bergeret, J.C. Bertolini, Chem. Eng. J. 107 (2005) 45–53.
[87] F.J.C.S. Aires, I. Kurzina, G.G. Cervantes, J.C. Bertolini, Catal. Today. 117 (2006) 518–524.
[88] F. Santos Aires, M. Treilleux, G. Fuchs, A. Hoareau, P. Melinon, B. Cabaud, Zeitschrift für Physik D Atoms Mol. Clusters 12 (1989) 149–152.
[89] F.J. Cadete Santos Aires, P. Sautet, G. Fuchs, J.-L. Rousset, P. Mélinon, Microsc. Microanal. Microstruct. 4 (1993) 441–452.
[90] A. Berthet, A.L. Thomann, F.J. Cadete Santos Aires, M. Brun, C. Deranlot, J.C. Bertolini, J.P. Rozenbaum, P. Brault, P. Andreazza, J. Catal. 190 (2000) 49–59.
[91] R. Mahfouz, F.J. Cadete Santos Aires, A. Brenier, B. Jacquier, J.C. Bertolini, Appl. Surf. Sci. 254 (2008) 5181–5190.
[92] J.L. Rousset, F.J. Cadete Santos Aires, F. Bornette, M. Cattenot, M. Pellarin, L. Stievano, A.J. Renouprez, Appl. Surf. Sci. 164 (2000) 163–168.
[93] R. Mahfouz, F.J. Cadete Santos Aires, A. Brenier, E. Ehret, M. Roumié, B. Nsouli, B. Jacquier, J.C. Bertolini, J. Nanopart. Res. 12 (2010) 3123–3136.
[94] J.L. Rousset, F.J. Cadete Santos Aires, B.R. Sekhar, P. Mélinon, B. Prevel, M. Pellarin, J. Phys. Chem. B 104 (2000) 5430–5435.
[95] D.W. Goodman, Catal. Lett. 99 (2005) 1–4.
[96] S. Schimpf, M. Lucas, C. Mohr, U. Rodemerck, A. Brückner, J. Radnik, H. Hofmeister, P. Claus, Catal. Today 72 (2002) 63–78.
[97] T.F. Garetto, A. Borgna, C.R. Apesteguía, in: B. Delmon, G.F. Froment (Eds.), Studies in Surface Science and Catalysis, Elsevier, 1994, pp. 369–376.
[98] A. Sárkány, O. Geszti, G. Sáfrán, Appl. Catal. A: Gen. 350 (2008) 157–163.
[99] J.H. Kang, E.W. Shin, W.J. Kim, J.D. Park, S.H. Moon, J. Catal. 208 (2002) 310–320.
[100] P. Weerachawanasak, O. Mekasuwandumrong, M. Arai, S.-I. Fujita, P. Praserthdam, J. Panpranot, J. Catal. 262 (2009) 199–205.
[101] P. Weerachawanasak, P. Praserthdam, J. Panpranot, J. Nanosci. Nanotechnol. 14 (2014) 3170–3175.
[102] C.R. Lederhos, J.M. Badano, M.E. Quiroga, P.C. L'Argentière, F. Coloma-Pascual, Química Nova 33 (2010) 816–820.
[103] C.R. Lederhos, M.J. Maccarrone, J.M. Badano, G. Torres, F. Coloma-Pascual, J.C. Yori, M.E. Quiroga, Appl. Catal. A: Gen. 396 (2011) 170–176.
[104] S. Somboonthanakij, O. Mekasuwandumrong, J. Panpranot, T. Nimmanwudtipong, R. Strobel, S. Pratsinis, P. Praserthdam, Catal. Lett. 119 (2007) 346–352.
[105] A.A. Gribb, J.F. Banfield, Am. Mineral. 82 (1997) 717–728.
[106] P.C. L'Argentière, E.A. Cagnola, M.E. Quiroga, D.A. Liprandi, Appl. Catal. A: Gen. 226 (2002) 253–263.